International Journal of Nanomedicine

Dovepress
open access to scientific and medical research

Open Access Full Text Article

ORIGINAL RESEARCH

Synthesis Of PEG-Coated, Ultrasmall, Manganese-Doped Iron Oxide Nanoparticles With High Relaxivity For T_1/T_2 Dual-Contrast Magnetic Resonance Imaging

This article was published in the following Dove Press journal:
International Journal of Nanomedicine

Shilin Xiao
Xian Yu
Liang Zhang
Ya Zhang
Weijie Fan
Tao Sun
Chunyu Zhou
Yun Liu
Yiding Liu
Mingfu Gong
Dong Zhang

Department of Radiology, Xinqiao Hospital, Army Medical University, Chongqing, People's Republic of China

Background: Beyond magnetic resonance imaging (MRI), which has been widely used clinically, molecular MRI (mMRI) can further provide qualitative and quantitative information at the cellular and molecular levels. However, the diagnostic accuracy may not be satisfactory via single-contrast mMRI due to some interferences in vivo. T_1/T_2 dual-contrast MRI using the same contrast agent (CA) could significantly improve the detection accuracy. Therefore, in this study, we fabricated poly(ethylene glycol) (PEG)-coated, manganese-doped iron oxide nanocomposites (Mn-IONPs@PEG) as T_1/T_2 dual-contrast CA, and evaluated its feasibility of T_1/T_2 dual-contrast MRI in vitro and in vivo.

Methods: Mn-IONPs were prepared by the thermal decomposition of iron-eruciate and manganese-oleate complexes and were coated with 1,2-Distearoyl-sn-glycero-3-phosphoethanolamine-N-(methoxy[polyethylene glycol]-2000) (DSPE-PEG 2000). The physicochemical properties and cytotoxicity of the Mn-IONPs were fully characterized, followed by MRI in vitro and in vivo.

Results: Ultrasmall 3 nm-sized nanoparticles were successfully prepared and were identified using transmission electron microscopy (TEM), high-resolution TEM, and X-ray diffraction. After coating with DSPE-PEG, the Mn-IONPs@PEG displayed excellent hydrophilicity and good biocompatibility. Due to the manganese-doping and PEG coating, the Mn-IONPs@PEG showed good relaxivity in vitro. Especially, the Mn-IONPs@PEG coated with DSPE-PEG following a mass ratio to Mn-IONPs of 1:20 showed harmonious longitudinal relaxivity (r_1 = 7.1 $mM^{-1}s^{-1}$) and transversal relaxivity (r_2 = 120.9 $mM^{-1}s^{-1}$), making it a better candidate for T_1/T_2 dual-contrast mMRI. After administrated via a caudal vein, the Mn-IONPs@PEG can induce significant enhancement in both T_1-weighted and T_2-weighted MR images and the time at 10 mins after injection was regarded as a suitable time for imaging because both the T_1 and T_2 enhancement were optimum at that time.

Conclusion: The obtained Mn-IONPs@PEG exhibited good r_1 and r_2 and was a reasonable candidate for T_1/T_2 dual-contrast mMRI.

Keywords: magnetic resonance imaging, manganese-doped iron oxide nanoparticles, T_1/T_2 dual-contrast, DSPE-PEG coating, high relaxivity

Correspondence: Mingfu Gong; Dong Zhang
Department of Radiology, Xinqiao Hospital, Army Medical University, Xinqiao Street, Shapingba District, Chongqing, People's Republic of China
Tel +86 23 6876 3843
Fax +86 23 6875 5306
Email hummer198625@163.com; hszhangd@163.com

Introduction

In recent decades, magnetic resonance imaging (MRI) has played an irreplaceable role in medical diagnosis because of its efficient soft tissue contrast, high spatial resolution, lack of ionizing radiation, and unrestricted signal penetration depth.[1,2]

submit your manuscript | www.dovepress.com
DovePress
http://doi.org/10.2147/IJN.S219749

Particularly, molecular magnetic resonance imaging (mMRI) has extended beyond traditional MRI technology. mMRI can obtain qualitative and quantitative information about biological processes in vivo at the cellular and molecular levels, greatly expanding the research and application fields of MRI.[3–5] In recent years, mMRI has been intensively studied in gene imaging,[6] cell tracing,[7] drug screening,[8] and evaluating early diagnoses and therapeutic effects of disease.[9,10] Contrast agent (CA) serving as the signal source of mMRI is the most important ingredient and has reasonably become a hot spot in the field of mMRI.[11]

Although many types of CA based on magnetic nanoparticles (NPs) with high longitudinal relaxivity (r_1)[12] or transverse relaxivity (r_2)[13] have been developed, single-contrast mMRI still possesses insufficient sensitivity and specificity due to its innate properties. Transverse relaxation time (T_2) single-contrast CA usually results in MR signal loss and susceptibility artifacts.[14] Additionally, the darker areas in MR T_2-weighted imaging (T_2WI) induced by the T_2 single-contrast CA may be confused with other physiological or pathological low-signal regions, such as bleeding, calcification, and metal deposition, which will significantly reduce the sensitivity and specificity of mMRI.[15] Similarly, some normal tissues (such as fatty tissue) with hyperintensity in MR longitudinal relaxation time (T_1)-weighted imaging (T_1WI) may be misunderstood as bright lesions enhanced by T_1 CA. T_1/T_2 dual-contrast MRI using the same CA provides complementary information about a lesion to self-confirm and provide fault-free MR images, proving that it can significantly improve the detection accuracy.[16,17]

Thus far, multifarious CAs have been reported for T_1/T_2 dual-contrast MRI. A common strategy for the synthesis of T_1/T_2 dual-contrast CA is to integrate T_1 and T_2 signal moieties as hybrid nanoparticles.[17–23] However, due to the magnetic coupling effect, the enhancement generated by the T_1 and T_2 moieties will interact with each other, leading to the compromise of both r_1 and r_2. Embedding the T_1 species into the T_2 species can parallel the electronic spins of paramagnetic T_1 CA with the direction of the magnetic field induced by the T_2 CA, and reasonably enhance both the T_1 and T_2 relaxivity of the T_1/T_2 dual-contrast CA.[16]

Because of good biocompatibility, high relaxivity, and easy and versatile functionalization, superparamagnetic iron oxide nanoparticles (IONPs) have been extensively studied and have emerged as promising T_2 CA.[24] Benefiting from the size-dependent contrast, the ultrasmall IONPs also have demonstrated satisfactory r_1, making them alternative T_1/T_2 dual-contrast CA.[25,26] Nevertheless, the increased T_1 relaxivity of the ultrasmall IONPs is the result of the consumption of the size, resulting in a relatively small r_2. Thus, ultrasmall IONPs may be not optimal as T_1/T_2 dual-contrast CA.

Divalent manganese ions (Mn^{2+}) possess five unpaired electrons and are of higher paramagnetism, and Mn^{2+} doping has been proven to be an effective route to improve the r_1 of ultrasmall IONPs.[12,27,28] Additionally, doped Mn^{2+} with a higher magnetic moment (μ_B=5.92) can occupy both the tetrahedral (T_d) and octahedral holes (O_h) in the crystal lattices, resulting in a special mixed spinel structure, a larger saturation magnetization (Ms), and a high r_2 of manganese-doped IONPs (Mn-IONPs).[2,29] Moreover, based on the embedding rationale, the doped Mn^{2+} and ultrasmall IONPs show synergetic enhancement, which will further improve both r_1 and r_2 of Mn-IONPs. Therefore, Mn-IONPs could be better candidates as dual-contrast CA.

Usually, the hydrophobic inorganic nanoparticles need to be modified with either natural macromolecules or synthetic polymers for hydrophilia and further functionalization for biomedical applications. 1,2-Distearoyl-sn-glycero-3-phosphoethanolamine-N-(methoxy [polyethylene glycol]) (DSPE-PEG), with various advantages such as a low critical micellar concentration (CMC), excellent biocompatibility, and long blood circulation time has been diffusely employed for surface modification. More importantly, it was reported that DSPE-PEG can significantly improve r_2 of the IONPs via the immobilization of nearby water molecules by forming hydrogen bonds.[30,31]

Herein, Mn-IONPs were prepared through the dynamic simultaneous thermal decomposition (DSTD) method. Strikingly, after coating with DSPE-PEG, the obtained hydrophilic manganese-doped iron oxide nanocomposites (Mn-IONPs@PEG) showed both good r_1 and r_2 in vitro and in vivo, demonstrating that these nanocomposites comprising ultrasmall Mn-IONPs and DSPE-PEG could be ideal candidates for use as T_1/T_2 dual-contrast CA.

Materials And Methods

Materials

Oleyl alcohol and dibenzyl ether were purchased from Aldrich Chemical Co. (Saint Louis, MO, USA). Absolute ethyl alcohol was obtained from Chongqing Chuandong Chemical Co. Ltd. (Chongqing, China). Hexane and tetrahydrofuran (THF) were purchased from Adamas Reagent Co. Ltd. (Shanghai, China). DSPE-PEG2000 was obtained

from Shanghai Ponsure Biotechnology Co. Ltd. (Shanghai, China). Dulbecco's Modified Eagle's Medium (DMEM) was purchased from Life Technologies Co. (Saint Louis, MO, USA). Fetal bovine serum (FBS) was obtained from Zhejiang Tianhang Biotechnology Co. Ltd. (Zhejiang, China). Penicillin/streptomycin solution and L-glutamine were purchased from Beyotime Biotechnology Co. Ltd. (Shanghai, China). Cell Count Kit-8 (CCK-8) was purchased from Boster Biological Technology Co. Ltd. (Wuhan, China). All of these reagents were used as received.

Synthesis Of Mn-IONPs

The Mn-IONPs were prepared following a previously reported procedure with modifications.[12] The iron-eruciate and manganese-oleate were first synthesized and described in the supporting information (SI) in detail. Next, 2 mmol of iron-eruciate, 1 mmol of manganese-oleate and 6 mmol of oleyl alcohol were dissolved in 10 mL of dibenzyl ether at room temperature. The mixture was then heated to 100 °C and maintained for 30 min under a constant argon flow and magnetic stirring. Subsequently, the mixture was heated to 265 °C at a rate of 5 °C/min and was maintained for 1 h. After cooling to room temperature, the synthesized Mn-IONPs were washed with ethanol and centrifuged and were finally dispersed in 20 mL of hexane for storage.

Surface Modification

By coating with the DSPE-PEG-2000, the Mn-IONPs were characterized with hydrophilia. Following the previous method,[32] 50 mg of Mn-IONPs was first dispersed in 50 mL of THF to form 1 mg/mL of Mn-IONPs solution. Next, DSPE-PEG-2000 was mixed with 1 mL of Mn-IONPs solution with different mass ratios (NPs/PEG = 1:1, 1:5, 1:20, or 1:40) and then was added dropwise into 5 mL of deionized water under ultrasonication. After shaking overnight, the supernatants, including Mn-IONPs@PEG (1:1, 1:5, 1:20, or 1:40), were collected via filtration through a 0.22-μm syringe filter and was stored at 4 °C. Additionally, the hydrophilic Mn-IONPs-TMAH were obtained through ligand exchange with tetramethylammonium hydroxide aqueous solution (TMAH) and were described in the SI in detail.

Characterization

Transmission electron microscopy (TEM; Hitachi HT-7700, Japan) was used to characterize the morphology of the nanoparticles. High-resolution transmission electron microscopy (HRTEM; FEI TECNAI G20, USA) was used to observe the lattice spacing of the nanoparticles. Powder X-ray diffraction (XRD; PANalytical X'Pert Powder, Netherlands) was performed to detect the structure of the nanoparticles. Inductive-coupled plasma optical emission spectrometry (ICP-OES; Thermo Scientific Icap6300 Duo, USA) was carried out to determine the elemental composition of the nanoparticles. The hysteresis loops of the nanoparticles were recorded using a superconducting quantum interference device (SQUID; VSM-Versalab, USA) magnetometer.

Cytotoxicity

The human liver carcinoma cell line HepG2, purchased from the Chinese Academy of Sciences Cell Bank, was used for cytotoxicity analysis in this study. The cells were routinely cultured in DMEM containing 10% FBS, 2 mM L-glutamine, and 100 U/mL penicillin/streptomycin solution in a humidified incubator with 5% CO_2 at 37 °C. CCK-8 was used for the analysis of the cytotoxicity of Mn-IONPs@PEG (1:20). Briefly, the cells were seeded in 96-well plates at a density of 1×10^4 cells/well and were cultured overnight. Next, fresh mediums containing Mn-IONPs@PEG with serial metal (Fe + Mn) concentrations (0, 1, 5, 10, 20, or 50 μg/mL) were added to replace the previous medium, followed by incubation for an additional 24 h. Each concentration of the samples was repeated five times. Next, the medium was replaced with 100 μL of fresh medium including 10 μL of WST-8 solution. Following 1.5 h of coculture, a spectral scanning multimode reader (Thermo Scientific Varioskan Flash, USA) was used to determine the optical density at the wavelength of 450 nm.

MR Imaging In Vitro

In vitro MR imaging was carried out using a clinical 3.0 T MRI scanner (GE, Signa HDx 3.0T, USA) with a head coil. The Mn-IONPs@PEG and Mn-IONPs-TMAH (shown in SI) solutions with [Fe+Mn] concentrations from 0 to 0.5 mM were imaged using the following parameters: fast spin echo sequence (FSE) T_1WI: repetition time (TR) = 240 ms, echo time (TE) = 7.5 ms, field of view (FOV) = 160×160 mm^2, matrix = 320×192, slice thickness/spacing =2.0 mm/0.1 mm, number of excitations (NEX) = 4; T_1 mapping: TE = 9 ms, TR = 150, 300, 600, 900, 1200 ms, FOV = 160×160 mm^2, matrix = 256×256, slice thickness/spacing = 2.0 mm/0.1 mm, NEX = 1; FSE T_2WI: TR = 2000 ms, TE = 46.5 ms, FOV = 160×128 mm^2, matrix = 192×160, slice thickness/spacing

= 2.0 mm/0.1 mm, NEX = 4; T_2 mapping: TR = 1500 ms, TE = 7.8, 15.6, 23.5, 31.3, 39.1, 46.9, 54.8, 62.6 ms, FOV = 160×128 mm^2, matrix = 160×128, slice thickness/spacing = 2.0 mm/0.4 mm, and NEX = 1.

MR Imaging In Vivo

Animal experiments were conducted in accordance with the National Institutes of Health guidelines on the use of animals in research and were approved by the Laboratory Animal Welfare and Ethics Committee of the Army Medical University. Female C57BL/6 mice with a body weight of approximately 20 g at the age of 8 weeks were purchased from Chongqing TengXin Biotechnology Co. and were housed at the Experimental Animal Center of XinQiao Hospital. The mice were anesthetized with isoflurane and were maintained in a stereotaxic frame (R510IP; RWD Life Science). The T_1WI (TE=9.3 ms, TR=580 ms, FOV = 60×60 mm^2, matrix = 288×192, slice thickness/spacing =2.0 mm/0 mm, and NEX = 4) and T_2WI (TE=69.6 ms, TR=2820 ms, FOV = 60×60 mm^2, matrix = 288×192, slice thickness/spacing =2.0 mm/0 mm, and NEX = 6.) Images of mice were acquired using a special rat coil (MS40; Suzhou Medcoil Healthcare Co., Ltd) and a 3.0-T clinical GE MRI scanner before and after injection of the Mn-IONPs@PEG (1:20) with 5 mg [Fe+Mn] per kilogram body weight.

Results

Synthesis And Characterization Of Mn-IONPs

Mn-IONPs were prepared via thermal decomposition of iron-eruciate and manganese-oleate complexes in the presence of oleyl alcohol in dibenzyl ether. Iron-eruciate and manganese-oleate complexes were manufactured through a simple method and are shown in Figure S1. The characteristic bands of iron-eruciate appeared at 1582, 1557, and 1433 cm^{-1}, while those of manganese-oleate were at 1606, 1549, and 1423 cm^{-1}, which were consistent with the data of a previous report.[12] The TEM images and corresponding distribution graphs of the obtained nanoparticles are shown in Figure 1A and B, showing that these nanoparticles were of a size 3.0 ± 0.28 nm with a narrow distribution and good uniformity. The crystal lattice fringes shown in the HRTEM images (Figure 1C and D) demonstrated the high crystallinity of the Mn-IONPs, and the measured interplanar distances of 2.56 and 2.97 Å were equivalent to the (311) and (220) lattice planes of Fe_3O_4, respectively. The XRD patterns are shown in Figure 1E. Compared with the spinel Fe_3O_4 powder diffraction data

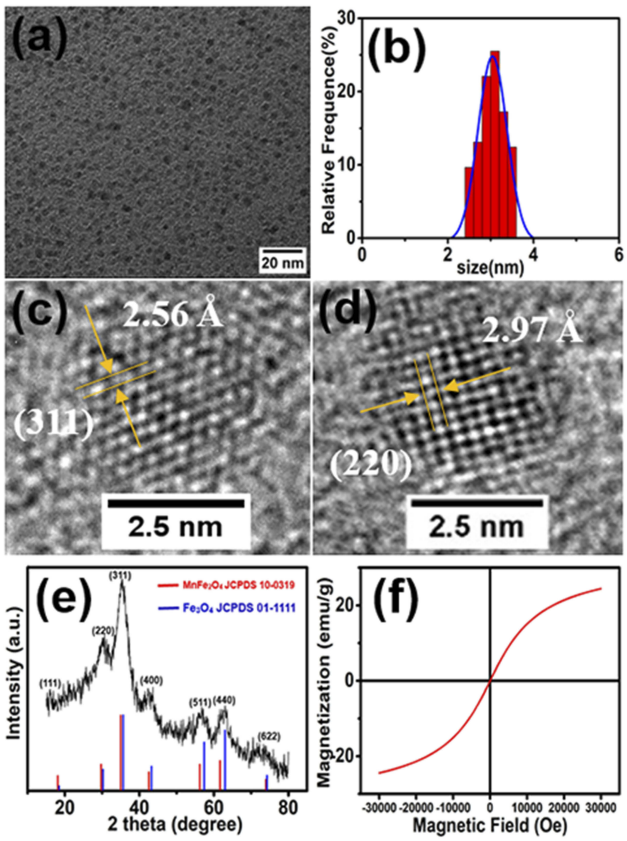

Figure 1 (**A**) TEM image, (**B**) size distribution graph, (**C, D**) HRTEM images, (**E**) XRD pattern, and (**F**) hysteresis loop of synthesized Mn-IONPs.

(JCPDS card no. 01–1111), these diffraction peaks shifted slightly toward that of $MnFe_2O_4$ (JCPDS card no. 10–0319), which can be attributed to the doped manganese. Coupled with the results of ICP-OES showing that the Mn/Fe molar ratio was approximately 0.20, Mn-IONPs were revealed to be successfully prepared. The hysteresis loop recorded by a SQUID magnetometer using a magnetic field up to 3.0 T at the temperature of 300 K showed that the saturation magnetization (Ms) of Mn-IONPs was 24.45 emu g^{-1} (Figure 1F). Meanwhile, the negligible coercivity and remanence when the external magnetic field was absent indicate their superparamagnetic behavior. Furthermore, after coating with DSPE-PEG-2000 or TMAH, the obtained hydrophilic Mn-IONPs@PEG or Mn-IONPs-TMAH still maintained size uniformity and showed good stability in water.

Relaxivity Of Mn-IONPs

To assess T_1 and T_2 enhancement, the Mn-IONPs@PEG and Mn-IONPs-TMAH solutions were imaged using a 3.0 T clinical MRI scanner with FSE T_1WI, FSE T_2WI, T_1 mapping and T_2 mapping sequences. The two types of Mn-IONPs solutions

all showed concentration-dependent signal enhancement (Figure 2A–D). With the concentration increasing, the signal intensity tended to be brighter in T_1WI but gradually grew darker in T_2WI. The linear fitting of the concentration and $1/T_1$ or $1/T_2$ showed that r_1 values of Mn-IONPs-TMAH, Mn-IONPs@PEG (1:1), Mn-IONPs@PEG (1:5), Mn-IONPs @PEG (1:20), and Mn-IONPs@PEG (1:40) were 3.7, 2.4, 3.5, 7.1, and 7.8 $mM^{-1}s^{-1}$, respectively (Figure 2E), and the r_2 values were 36.9, 199.5, 149.7, 120.9, and 94.8 $mM^{-1}s^{-1}$, respectively (Figure 2F).

In Vitro Cytotoxicity Assay

Excellent biocompatibility was considered to be an important requirement of Mn-IONPs@PEG for in vivo

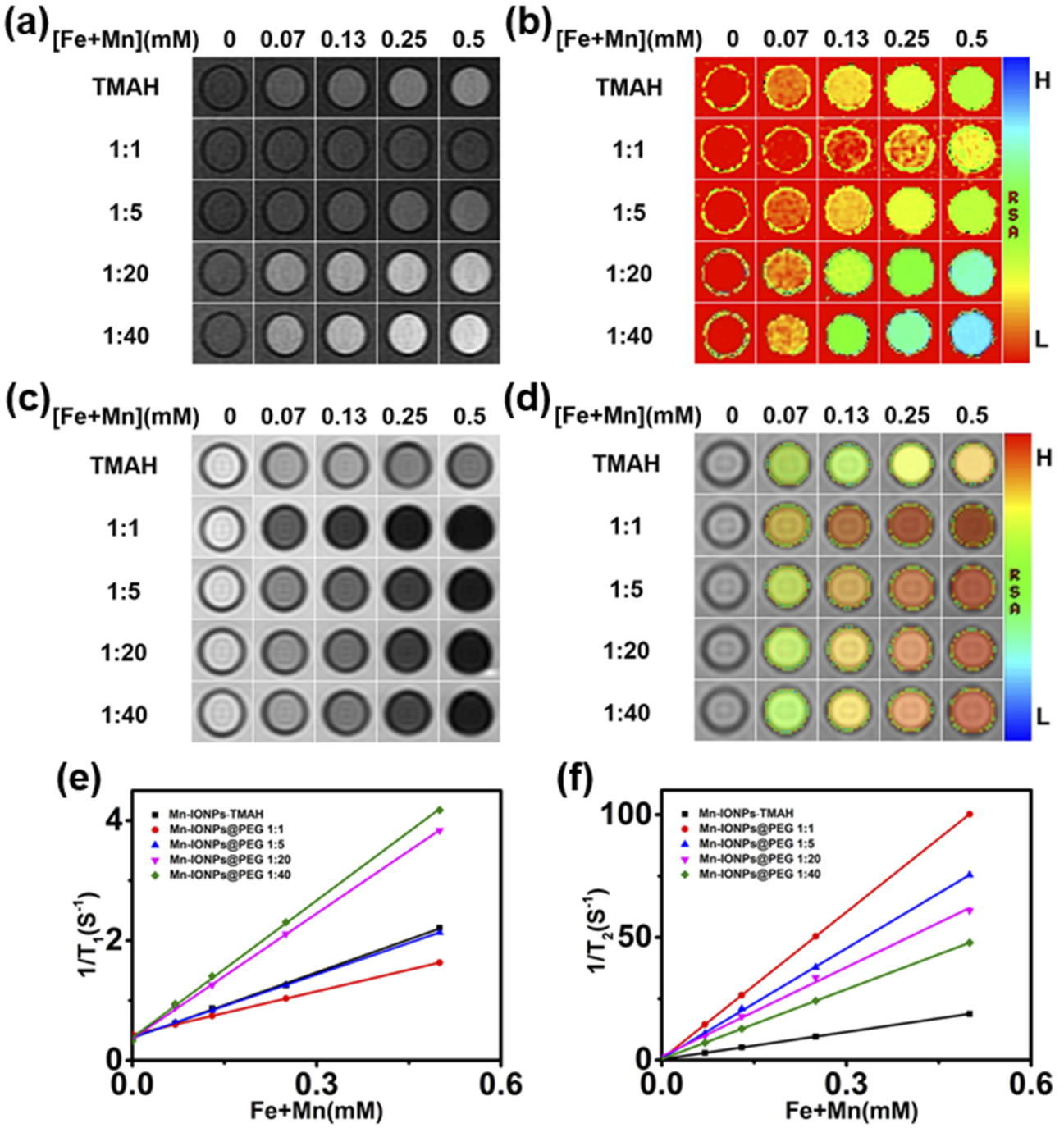

Figure 2 In vitro MR images of the Mn-IONPs-TMAH and Mn-IONPs@PEG (1:1, 1:5, 1:20, and 1:40) at 3.0 T: (**A**) T_1-weighted, (**B**) T_1 mapping, (**C**) T_2-weighted and (**D**) T_2 mapping. (**E, F**) Linear fitting of $1/T_1$ and $1/T_2$ over different (Fe+Mn) concentrations of the nanocomposites.

application. The in vitro cell cytotoxicity assay of Mn-IONPs@PEG (1:20) was performed on HepG2 cells using CCK-8. Figure 3 shows the viability of HepG2 cells co-cultured with the Mn-IONPs@PEG of [Fe+Mn] concentration ranging from 1 to 50 μg/mL at 37 °C for 12 hrs and 24 hrs. All the cells survived under the current experimental conditions. All Mn-IONPs@PEG samples showed insignificant toxicity with a cell viability greater than 80% at a concentration of less than 50 μg/mL for 12 hrs and 24 hrs. These results demonstrated that Mn-IONPs@PEG have a good biocompatibility.

In Vivo Contrast-Enhanced MRI

Based on the above results, we further explored the potential of the Mn-IONPs as dual-contrast CA in vivo. Due to the high relaxivity, Mn-IONPs@PEG (1:20) were employed for contrast-enhanced MRI of the liver. Figure 4A shows the axial T_1WI and T_2WI MR images acquired preinjection and postinjection (0, 10, 30, 60, and 120 min) of Mn-IONPs@PEG. The significantly brighter T_1WI MR images and darker T_2WI MR images suggest good r_1 and r_2 values of Mn-IONPs@PEG in vivo. The contrast-enhancement ratios of the MR signal intensity ΔSI ($\Delta SI = (SI_{post} - SI_{pre})/SI_{pre} \times 100\%$) are shown in Figure 4B and C. The ΔSI peak of 133% in T_1WI appeared at 10 min after injection followed by a gradual decrease, unexpectedly becoming negative at 120 min. By contrast, the T_2WI images showed obvious enhancement at 10 min after injection but increased to a plateau at 30 min and maintained for a long period.

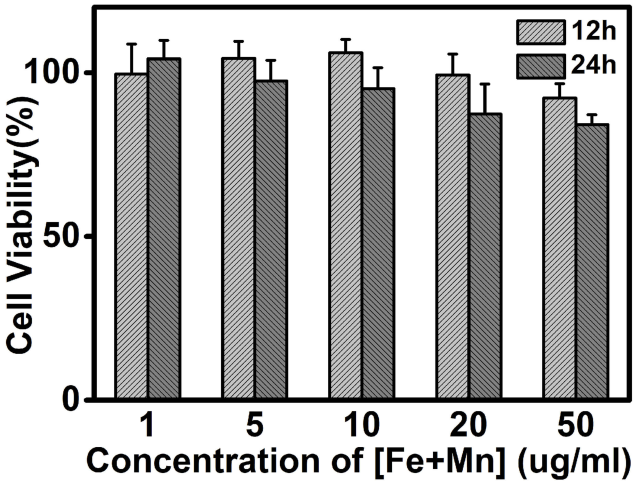

Figure 3 Viability of HepG2 cells after incubation with Mn-IONPs@PEG (1:20) at different concentrations (1–50 μg/mL of [Fe+ Mn]) at 37 °C for 12 hrs and 24 hrs.

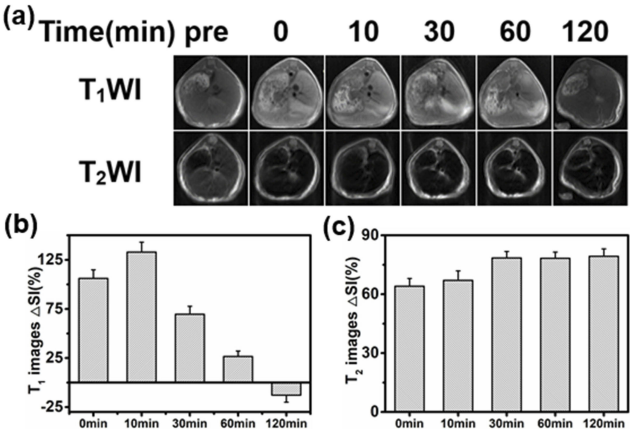

Figure 4 (**A**) T_1-weighted and T_2-weighted MR images of transverse planes of the liver using the FSE sequence acquired at 0, 10, 30, 60, or 120 min after intravenous administration of Mn-IONPs@PEG (1:20). (**B, C**) Enhancement ratio of the MR signal ΔSI of the liver after contrast-enhancement by Mn-IONPs@PEG (1:20).

Discussion

As is well known, T_1 enhancement of superparamagnetic NPs depends on the interaction of the paramagnetic ions on the surface and nearby proton. Doping paramagnetic ions into the NPs has proven to be an effective route to improve r_1.[29] Many kinds of metal ions have been reported to be paramagnetic because of their unpaired electrons. Unlike lanthanide ions, the transition metal ions show both excellent biocompatibility and comparative paramagnetism and should be considered better ions for doping. Mn^{2+} with five unpaired electrons shows the highest paramagnetism compared with other transition metal ions.[2] Additionally, based on the quantum mechanical inner-sphere theory, the T_1 relaxivity for NPs-based T_1 CA can be given by[33]

$$\frac{1}{T_1} = \frac{qP_M}{T_{1M} + \tau_M} \quad (1)$$

where P_M is the mole fraction of metal ions, q is the number of water molecules bound per metal ion, τ_M is the residence lifetime of the bound water, and T_{1M}, which is related to τ_M and the rotational correlation time (τ_R), is the relaxation time of the bound water protons. It was revealed that the τ_M of Mn $(H_2O)_6^{2+}$ is 4.3×10^4 ns and is 2 orders of magnitude smaller than that of $Fe(H_2O)_6^{3+}$ (5.3×10^6 ns) and other transition metal ions.[33] Thus, Mn^{2+} doping will effectively accelerate spin-lattice relaxation and increase r_1. Moreover, embedding paramagnetic ions into the superparamagnetic NPs significantly boosts both r_1 and r_2 of superparamagnetic hybrid NPs by synergetic interaction between the T_1 and T_2 species.[16]

In addition to Mn^{2+} doping, decreasing the size of NPs into the ultrasmall region has also been proven to be an effective approach to boost r_1. The smaller the size of

superparamagnetic NPs is, the larger the surface-to-volume ratio is, and the more superficial paramagnetic ions are, and the better r_1 the NPs possess.[12] Thus, sufficiently small Mn^{2+} doping nanoparticles must be synthesized to guarantee good r_1. Theoretically, the key to successfully obtain ultrasmall Mn^{2+} doping nanoparticles is to decompose both the precursors at a similar temperature to form a multiple metal-containing monomer before nucleation to obtain smaller nanoparticles instead of a single-metal-containing monomer, resulting in the formation of a nondopant-containing nucleus initially and then another metal serving as the host to grow nanoparticles.[12] Thus, the Mn-IONPs in this study were prepared by DSTD of the iron-eruciate and manganese-oleate complexes, which had a similar decomposition temperature in the presence of oleyl alcohol in dibenzyl ether instead of iron (III) acetylacetonate and manganese (II) acetylacetonate. From the results of TEM, HRTEM, XRD and ICP, Mn-IONPs with an ultrasmall size of 3.0 ± 0.28 nm were successfully synthesized and the Mn^{2+} was fully proven to be doped successfully.

It is very important to have both good r_1 and r_2 to be good T_1/T_2 dual-contrast CA. However, we decreased the size of the NPs to the ultrasmall range to reach an optimal r_1 of the NPs in this study, resulting in a relative thicker spin-canted layer and a much lower saturation magnetization (*Ms*) and, finally, a much lower r_2 as expected. Unlike r_1, the relaxation of T_2 CA is dominated by the outer-sphere mechanism and can be given by[34]

$$\frac{1}{T_2} = \frac{256\pi^2\gamma_I M_n}{1215\rho}\left(\frac{1}{1+L/a}\right)^3 Ms^2\tau_D \qquad (2)$$

where γ_I, M_n, ρ, a and L are the proton gyromagnetic ratio, molar mass, density, radius of NPs and impermeable thickness of the surface coating layer, respectively. τ_D is the translational diffusion time, which is determined by r and D according to the equation $\tau_D = r^2/D$, where r and D are the effective radius and diffusion coefficient, respectively. It is obvious that r_2 is proportional to a^3, while Ms^2 and τ_D are inversely proportional to L^3. To increase *Ms*, we doped Mn^{2+} into ultrasmall supermagnetic magnetite. Because the doped Mn^{2+} can occupy both the tetrahedral (T_d) and octahedral holes (O_h) in the crystal lattices, Mn-IONPs form a special mixed spinel structure, finally resulting in larger *Ms* and r_2; this finding has been confirmed in this study by showing that the r_2 of Mn-IONPs-TMAH (36.9 $mM^{-1}s^{-1}$) is larger than IONPs with the same size (r_2 = 29.2 $mM^{-1}s^{-1}$).[15] Using another approach by coating Mn-IONPs with DSPE-PEG, we further enhance its r_2.

According to Equation (2), r_2 can be improved by decreasing D. The PEG molecules on the surface of the Mn-IONPs can immobilize surrounding water molecules in a large region by forming hydrogen bonds, resulting in a small D and a large τ_D.[30,31] Thus, it is reasonable that all the DSPE-PEG-coated Mn-IONPs showed a much higher r_2 than THAM-coated Mn-IONPs. However, a decreasing trend for r_2 was noted with the increase in the molar ratio of Mn-IONPs: DSPE-PEG. This phenomenon can be easily explained because the hydrogen–bond interactions between PEG and water protons have a critical molar ratio. Too many coating molecules may exclude water protons from the induced magnetic field from the Mn-IONPs, forming an impermeable coating layer on the surface of the Mn-IONPs and leading to a lower r_2. Interestingly, we also found that r_1 can be changed by varying the coating molecules and the molar ratio of these molecules. Mn-IONPs-TMAH showed a higher r_1 than Mn-IONPs-PEG (1:1) and Mn-IONPs-PEG (1:5) but possessed a lower r_1 than Mn-IONPs-PEG (1:20) and Mn-IONPs-PEG (1:40). Unlike r_2, r_1 increased significantly with the increase in the molar ratio of Mn-IONPs: DSPE-PEG. This phenomenon can be attributed to τ_R and q based on Equation (1). As is well known, T_1 relaxation relies on a chemical exchange between the paramagnetic center and water molecules in the first coordination sphere. The more water molecules located in the first coordination sphere, the better r_1 is. Although NPs become hydrophilic by coating with DSPE-PEG, there is still a DSPE-oleic acid layer that is impermeable on the surface of the NPs, resulting in much fewer water molecules in the first coordination sphere than Mn-IONPs-TMAH, in which the impermeable oleic acid layer has been exchanged. Thus, the r_1 of Mn-IONPs-TMAH was higher than that of Mn-IONPs-PEG (1:1) and Mn-IONPs-PEG (1:5). However, why do Mn-IONPs-PEG (1:20) and Mn-IONPs-PEG (1:40) show a higher r_1 than Mn-IONPs-TMAH? The cause may be that r_1 can also be remarkably influenced by τ_R, which is proportional to the molecular weight. With the increase in the molar ratio of Mn-IONPs: DSPE-PEG, the molecular weight of NPs increases notably, leading to a higher r_1. Over the critical ratio, the shielding effect of the impermeable DSPE-oleic acid layer will be counteracted and τ_R will be dominant, making the r_1 of Mn-IONPs-PEG (1:20) and Mn-IONPs-PEG (1:40) higher than that of Mn-IONPs-TMAH.

Excellent biocompatibility is considered a key point for inorganic NPs application in vivo.[11] To improve the biocompatibility, we selected DSPE-PEG, a well-established nonimmunogenic and noncytotoxic material, for Mn-IONPs coating. By CCK-8 analysis, the acquired Mn-IONPs@PEG (1:20) showed negligible cytotoxicity and excellent biocompatibility, which were consistent with the results of previous studies.[30,31,35] Thus, we further explored the potential of Mn-IONPs@PEG (1:20) for T_1/T_2 dual-contrast MR imaging in vivo. Obviously, clear signal intensity changes were noted in both T_1WI and T_2WI over time. The signal intensity changes in the liver may be the result of the biological distribution and metabolism of Mn-IONPs@PEG in vivo. After injection, Mn-IONPs@PEG gradually accumulated in the liver within 10 mins, leading to increased ΔSI of both T_1 and T_2. However, the ΔSI of T_1WI decreased over time because of passive aggregation driven by the phagocytosis of Kupffer cells, resulting in stable and individual Mn-IONPs@PEG gradually aggregating into clusters and causing the larger T_2 contrast enhancement compared with the smaller T_1 contrast enhancement. Particularly, the ΔSI even turned out to be negative at 120 min because the dominated T_2 contrast enhancement significantly affected the T_1 contrast. By contrast, the ΔSI of T_2WI kept increasing until it reached a plateau and there was no downward trend within the observation period because of no degradation. The results obtained from the in vivo MRI verified that Mn-IONPs@PEG are highly sensitive T_1 and T_2 dual CA for imaging of the liver.

Conclusion

In summary, we successfully synthesized 3-nm-sized Mn-IONPs via facile thermal decomposition of iron-eruciate and manganese-oleate complexes in the presence of oleyl alcohol in dibenzyl ether. After encapsulation in DSPE-PEG-2000, the Mn-IONPs@PEG displayed good colloidal stability and excellent biocompatibility. More importantly, due to Mn^{2+} doping and DSPE-PEG-2000 coating, the synthesized NPs showed unexpected high r_1 and r_2. Confirmed by in vitro and in vivo MR imaging, the Mn-IONPs@PEG are ideal candidates for use as T_1/T_2 dual-contrast CA.

Acknowledgment

This research was supported by National Science Foundation of China (No. 81471635 and 81501521), Natural Science Foundation of Chongqing (No. cstc2018jcyjAX0321 and cstc2017jcyjBX0038).

Disclosure

The authors report no conflicts of interest in this work.

References

1. Smith BR, Gambhir SS. Nanomaterials for in vivo imaging. *Chem Rev*. 2017;117(3):901–986. doi:10.1021/acs.chemrev.6b00073
2. Ni D, Bu W, Ehlerding EB, et al. Engineering of inorganic nanoparticles as magnetic resonance imaging contrast agents. *Chem Soc Rev*. 2017;46(23):7438–7468. doi:10.1039/c7cs00316a
3. Weissleder R. Molecular imaging in cancer. *Science*. 2006;312:1168–1171.
4. Weissleder R. Molecular imaging: exploring the next frontier. *Radiology*. 1999;212(3):609–614.
5. Herschman HR. Molecular imaging: looking at problems, seeing solutions. *Science*. 2003;302(5645):605–608.
6. Louie AY, Hüber MM, Ahrens ET, et al. In vivo visualization of gene expression using magnetic resonance imaging. *Nat Biotechnol*. 2000;18:321.
7. Liu J, Wang L, Cao J, et al. Functional investigations on embryonic stem cells labeled with clinically translatable iron oxide nanoparticles. *Nanoscale*. 2014;6(15):9025–9033.
8. Willmann JK, van Bruggen N, Dinkelborg LM, Gambhir SS. Molecular imaging in drug development. *Nat Rev Drug Discov*. 2008;7(7):591–607.
9. Yang Z, Ren J, Ye Z, et al. Bio-inspired synthesis of PEGylated polypyrrole@polydopamine nanocomposite as theranostic agent for t_1-weighted MR imaging guided photothermal therapy. *J Mater Chem B*. 2017;5:1108–1116.
10. Zhang F, Ni Q, Jacobson O, et al. Polymeric nanoparticles with a glutathione-sensitive heterodimeric multifunctional prodrug for in vivo drug monitoring and synergistic cancer therapy. *Angew Chem Int Ed Engl*. 2018;57(24):7066–7070. doi:10.1002/anie.201801984
11. Na HB, Song IC, Hyeon T. Inorganic nanoparticles for MRI contrast agents. *Adv Mater*. 2009;21(21):2133–2148. doi:10.1002/adma.v21:21
12. Zhang H, Li L, Liu XL, et al. Ultrasmall ferrite nanoparticles synthesized via dynamic simultaneous thermal decomposition for high-performance and multifunctional T_1 magnetic resonance imaging contrast agent. *ACS Nano*. 2017;11(4):3614–3631. doi:10.1021/acsnano.6b07684
13. Jang JT, Nah H, Lee JH, et al. Critical enhancements of MRI contrast and hyperthermic effects by dopant-controlled magnetic nanoparticles. *Angew Chem Int Ed Engl*. 2009;48(7):1234–1238. doi:10.1002/anie.200805149
14. Shin T-H, Choi J-S, Yun S, et al. T_1 and T_2 dual-mode MRI contrast agent for enhancing accuracy by engineered nanomaterials. *ACS Nano*. 2014;8:3393–3401. doi:10.1021/nn405977t
15. Kim BH, Lee N, Kim H, et al. Large-scale synthesis of uniform and extremely small-sized iron oxide nanoparticles for high-resolution T_1 magnetic resonance imaging contrast agents. *J Am Chem Soc*. 2011;133(32):12624–12631. doi:10.1021/ja203340u
16. Zhou Z, Huang D, Bao J, et al. A synergistically enhanced T_1-T_2 dual-modal contrast agent. *Adv Mater*. 2012;24(46):6223–6228. doi:10.1002/adma.201203169
17. Li J, You J, Wu C, et al. T_1-T_2 molecular magnetic resonance imaging of renal carcinoma cells based on nano-contrast agents. *Int J Nanomedicine*. 2018;13:4607–4625. doi:10.2147/IJN.S168660
18. Im GH, Kim SM, Lee DG, et al. Fe_3O_4/MnO hybrid nanocrystals as a dual contrast agent for both T_1- and T_2-weighted liver MRI. *Biomaterials*. 2013;34(8):2069–2076. doi:10.1016/j.biomaterials.2012.11.054
19. Tegafaw T, Xu W, Ahmad MW, et al. Dual-mode T_1 and T_2 magnetic resonance imaging contrast agent based on ultrasmall mixed gadolinium-dysprosium oxide nanoparticles: synthesis, characterization, and in vivo application. *Nanotechnology*. 2015;26(36):365102. doi:10.1088/0957-4484/26/36/365102

20. Yang M, Gao L, Liu K, et al. Characterization of $Fe_3O_4/SiO_2/Gd_2O(CO_3)_2$ core/shell/shell nanoparticles as T_1 and T_2 dual mode MRI contrast agent. *Talanta*. 2015;131:661–665. doi:10.1016/j.talanta.2014.08.042
21. Sun X, Du R, Zhang L, et al. A pH-responsive yolk-like nanoplatform for tumor targeted dual-mode magnetic resonance imaging and chemotherapy. *ACS Nano*. 2017;11(7):7049–7059. doi:10.1021/acsnano.7b02675
22. Cabrera-Garcia A, Checa-Chavarria E, Pacheco-Torres J, et al. Engineered contrast agents in a single structure for T_1-T_2 dual magnetic resonance imaging. *Nanoscale*. 2018;10(14):6349–6360. doi:10.1039/C7NR07948F
23. Gong M, Yang H, Zhang S, et al. Targeting T_1 and T_2 dual modality enhanced magnetic resonance imaging of tumor vascular endothelial cells based on peptides-conjugated manganese ferrite nanomicelles. *Int J Nanomedicine*. 2016;11:4051–4063.
24. Lee N, Hyeon T. Designed synthesis of uniformly sized iron oxide nanoparticles for efficient magnetic resonance imaging contrast agents. *Chem Soc Rev*. 2012;41(7):2575–2589.
25. Wang G, Zhang X, Skallberg A, et al. One-step synthesis of water-dispersible ultra-small Fe_3O_4 nanoparticles as contrast agents for T_1 and T_2 magnetic resonance imaging. *Nanoscale*. 2014;6(5):2953–2963.
26. Pellico J, Ruiz-Cabello J, Fernandez-Barahona I, et al. One-step fast synthesis of nanoparticles for MRI: coating chemistry as the key variable determining positive or negative contrast. *Langmuir*. 2017;33(39):10239–10247.
27. Li Z, Wang SX, Sun Q, et al. Ultrasmall manganese ferrite nanoparticles as positive contrast agent for magnetic resonance imaging. *Adv Healthc Mater*. 2013;2(7):958–964.
28. Zhang M, Cao Y, Wang L, et al. Manganese doped iron oxide theranostic nanoparticles for combined T_1 magnetic resonance imaging and photothermal therapy. *ACS Appl Mater Interfaces*. 2015;7(8):4650–4658.
29. Lee JH, Huh YM, Jun YW, et al. Artificially engineered magnetic nanoparticles for ultra-sensitive molecular imaging. *Nat Med*. 2007;13(1):95–99.
30. Tong S, Hou S, Zheng Z, et al. Coating optimization of superparamagnetic iron oxide nanoparticles for high T_2 relaxivity. *Nano Lett*. 2010;10(11):4607–4613.
31. LaConte LE, Nitin N, Zurkiya O, et al. Coating thickness of magnetic iron oxide nanoparticles affects R_2 relaxivity. *J Magn Reson Imaging*. 2007;26(6):1634–1641.
32. Lu J, Ma S, Sun J, et al. Manganese ferrite nanoparticle micellar nanocomposites as MRI contrast agent for liver imaging. *Biomaterials*. 2009;30(15):2919–2928.
33. RB LAUFFER. Paramagnetic metal complexes as water proton relaxation agents for NMR imaging theory and design. *Chem Rev*. 1987;87:901–927.
34. Zeng J, Jing L, Hou Y, et al. Anchoring group effects of surface ligands on magnetic properties of Fe_3O_4 nanoparticles: towards high performance MRI contrast agents. *Adv Mater*. 2014;26(17):2694–2698. 2016.
35. Johnson NJ, He S, Nguyen Huu VA, Almutairi A. Compact micellization: a strategy for ultrahigh t_1 magnetic resonance contrast with gadolinium-based nanocrystals. *ACS Nano*. 2016;10(9):8299–8307.